UNIVERSITY OF BRISTOL

Mustafa, A., Pedone, E., Marucci, L., Moschou, D., & Di Lorenzo, M. (2021). A Flow-through Microfluidic Chip for Continuous Dielectrophoretic Separation of Viable and Non-viable Human T-cells. *Electrophoresis*, 1-8. https://doi.org/10.1002/elps.202100031

## University of Bristol - Explore Bristol Research
### General rights

**Adil Mustafa**[1,2,6] (ORCID)
**Elisa Pedone**[3,5] (ORCID)
**Lucia Marucci**[3,5] (ORCID)
**Despina Moschou**[2,4] (ORCID)
**Mirella Di Lorenzo**[1,2] (ORCID)

[1]Department of Chemical Engineering, University of Bath, Bath, UK
[2]Centre for Biosensors, Bioelectronics and Biodevices, University of Bath, Bath, UK
[3]Department of Engineering Mathematics, University of Bristol, Bristol, UK
[4]Department of Electrical and Electronic Engineering, University of Bath, Bath, UK
[5]School of Cellular and Molecular Medicine, University of Bristol, Bristol, UK
[6]Current address: Department of Engineering Mathematics, University of Bristol, Bristol, UK

## Research Article

# A flow-through microfluidic chip for continuous dielectrophoretic separation of viable and non-viable human T-cells

Effective methods for rapid sorting of cells according to their viability are critical in T cells based therapies to prevent any risk to patients. In this context, we present a novel microfluidic device that continuously separates viable and non-viable T-cells according to their dielectric properties. A dielectrophoresis (DEP) force is generated by an array of castellated microelectrodes embedded into a microfluidic channel with a single inlet and two outlets; cells subjected to positive DEP forces are drawn toward the electrodes array and leave from the top outlet, those subjected to negative DEP forces are repelled away from the electrodes and leave from the bottom outlet. Computational fluid dynamics is used to predict the device separation efficacy, according to the applied alternative current (AC) frequency, at which the cells move from/to a negative/positive DEP region and the ionic strength of the suspension medium. The model is used to support the design of the operational conditions, confirming a separation efficiency, in terms of purity, of 96% under an applied AC frequency of $1.5 \times 10^6$ Hz and a flow rate of 20 µl/h. This work represents the first example of effective continuous sorting of viable and non-viable human T-cells in a single-inlet microfluidic chip, paving the way for lab-on-a-chip applications at the point of need.

Additional supporting information may be found online in the Supporting Information section at the end of the article.

## 1 Introduction

Cancer immunotherapy has demonstrated great potential for personalized therapies in both pre-clinical and clinical trials [1]. A successful example is the chimeric antigen receptor (CAR)-modified T-cells therapy, recently approved by American and European agencies (FDA and EMA, respectively) [2,3]. CAR-T cells, obtained by genetically engineering a patient's own T-cells, synergize with the endogenous immune response and specifically target tumor cells. The implementation of this promising therapy is, however, challenged by the manufacturing of clinical-grade CAR-T cells, which is currently costly and time consuming [4]. The search for alternative manufacturing strategies for CAR-T cells, compatible with lab-on-a-chip solutions, is, therefore, a critical focus in

the research community to generate point-of-care solutions that are much more affordable and practical to implement. Genetic engineering by electroporation allows for faster, safer, and cheaper nucleic acids transfer in T-cells over the traditionally used viral vectors [5]. This method, however, poses great risks of loss in cell viability due to the high magnitude of the applied electric field [5,6]. Prior to possible injection into the patient's body, it is therefore important to efficiently separate viable from non-viable CAR-T cells, as non-viable CAR-T cells can pose severe risks to the patient's health [7,8]. Traditionally, this separation is done under static conditions in a petri dish by using cell viability assays that measure cellular metabolic activity [9]. These assays are not only time consuming and laborious, but they are also characterized by low throughput [10,11]. Fluorescence-activated cell sorting (FACS) that uses flow cytometry can instead allow high-throughput cell separation or sorting [12,13]. This method requires sample pre-treatment, as the cells must be stained with a fluorescent dye, and an integrated light source [14]. Overall, these techniques for cell separation

---

**Correspondence**: Dr. Mirella Di Lorenzo, Chemical Engineering, University of Bath, BA2 7AY, Bath, UK
E-mail: m.di.lorenzo@bath.ac.uk

**Abbreviations: CAR-T**, chimeric antigen receptor modified T-cells; **CFD**, computational fluid dynamic; **MFI**, median fluorescence intensity; **PMP**, plasma membrane potential

**Color online**: See article online to view Figs. 1 and 2 in color.

require large sample volumes and are not compatible with a point-of-care therapeutics approach.

Alternatively, several microfluidic techniques have been reported for sorting viable and non-viable cells to address an increasing need for portability [15]. Most of these methods are based on the exploitation of physicochemical differences, involving the use of: hydrodynamic forces [16]; acoustic forces [17,18]; magnetophoretic forces [19,20]; inertial forces [21–23]; and membrane deformation [24]; fluorescence [25,26]; and differences in cell size [27]. A purity as high as 93% was obtained in the case of a separation based on hydrodynamic forces [16], where the separation efficiency is based on the difference in particle size. When acoustic forces are applied, the separation efficacy is a function of the applied voltage and the concentration of the cells in the suspension medium, and efficiencies in the range of 50–98% have been observed [17]. Similarly, separation efficiencies of 95% and 94% have been observed in the case respectively of the use of magnetophoretic forces [28] and inertial microfluidic forces [29]. Devices that exploit cell membrane stiffness to sort viable and non-viable cells have instead a lower sorting efficiency, which is in the range of 82–86% [24].

Among these methods, dielectrophoresis (DEP), a label-free separation technique that exploits the difference in dielectric properties of viable and non-viable cells, is particularly attractive, as it is a fast and cost-effective label-free analytical technique [30,31]. With DEP, cells are subjected to a non-uniform electric field [32] and move toward the high electric field region (positive DEP, pDEP) or away from it (negative DEP, nDEP), depending on whether they are more or less polarisable than the suspending medium [33,34]. DEP-based microfluidic devices for viable, and non-viable cell sorting, previously reported, can be categorized according to device design, electrode configuration, and operating parameters (applied frequency, and voltage), as summarized in Table S1. To minimize adverse effects caused by the electrochemical reactions onto the electrode surface, a reservoir-based dielectrophoretic (rDEP) microfluidic device for sorting viable and non-viable yeast cells was recently reported [35,36]. On the other hand, the use of interdigitated electrodes led to separation efficiency by DEP as high as 90% in microfluidic devices [37,38]. Open and closed channel Deterministic Lateral Displacement (DLD) microfluidic devices have also recently made use of DEP forces to sort cells based on both size and dielectric differences [39,40]. Zhao et al. [41] reported a three-inlet microfluidic device with asymmetric orifices embedding electrodes. In this device, the separation of live and dead yeast cells was achieved via a non-uniform electric field gradient over a large range of AC frequency spectrum. A two-inlet microfluidic device that combines electroporation with DEP-based sorting of viable cells has also been reported [42]; in this device, the second inlet is used to flow focus the cells to the center of the channel. Two arrays of microelectrodes fabricated in castellated configuration, and integrated within a microfluidic channel to generate opposing electric fields on both sides of the channel, have also been tested for DEP-based cell sorting [43,44]. In this setup, the

ratio of the opposing electric fields controls the cell position and sorting in the microchannels. Finally, Piacentini et al. [45] modified the castellated device design by using only one array of microelectrodes rather than two, in combination with hydrodynamic focusing, requiring a second inlet, to separate platelets from red blood cells with an efficiency of 97%.

In this work, we report the first DEP-based single-inlet microfluidic device custom-made for personalized cell therapy applications, to separate viable human T-cells (CD8$^+$) from non-viable T-cells based on their dielectric properties. Contrary to other devices so far reported, the system is characterized by a single inlet and separates the cells by applying an AC electric field via a single array of castellated microelectrodes. Consequently, the chip developed in this study has a simpler design and is compatible with continuous operations, with no need for additional reagents. The difference in the membrane potential of viable and non-viable human T-cells is assessed by flow cytometry using a voltage-sensitive dye (FloVolt). The cell sorting efficacy of the device is initially numerically investigated by using the dielectric properties of live and dead human T-cells as a function of ionic concentrations of suspending solution. Furthermore, the effect of both the applied AC frequency and flow rate on cell sorting efficiency is also quantified. The critical frequency for successful sorting viable and non-viable T-cells is consequently determined. To the best of our knowledge, this is the first example of effective sorting of viable and non-viable T-cells, based on their dielectric properties, via a microfluidic chip.

## 2    Mathematical model

To verify the working parameters of the microfluidic cell sorter, Computational Fluid Dynamic (CFD) studies were performed with COMSOL Multiphysics 5.5 (AC/DC, Microfluidics, and Particle tracing modules), using a double shell model for the Maxwell-Wagner interfacial polarization of mammalian cells. The model was tested by using the dielectric properties of T-cells reported in the literature [46–48], which are summarised in Table S2.

In the simulation, the electric current module was used to apply a complex AC electric field phasor in the frequency domain to the particles entering the microfluidic channel. The microfluidics module was used to establish creeping flow (Re < 1) for the particle movement. The particle tracing module was used to release particles into the separation region and to trace the particles as they migrate from inlet to outlet through the separation region. Moreover, the particle tracing module was used to apply drag and DEP force [49].

The CFD simulations were set up by feeding viable and non-viable cells with a ratio of 1:1. Two sets of CFD studies were solved. First, a parametric sweep of fluid medium conductivity, within the range of 0.02 S/m to 1 S/m, was performed by keeping the applied frequency, f (Hz), constant at a value of 1.5 × 10$^6$ Hz. Secondly, a parametric sweep of applied frequency, within the range of 1.5 × 10$^2$ Hz to 1.5 × 10$^{14}$ Hz, was performed by keeping the value of the

**(A)**



**(B)**
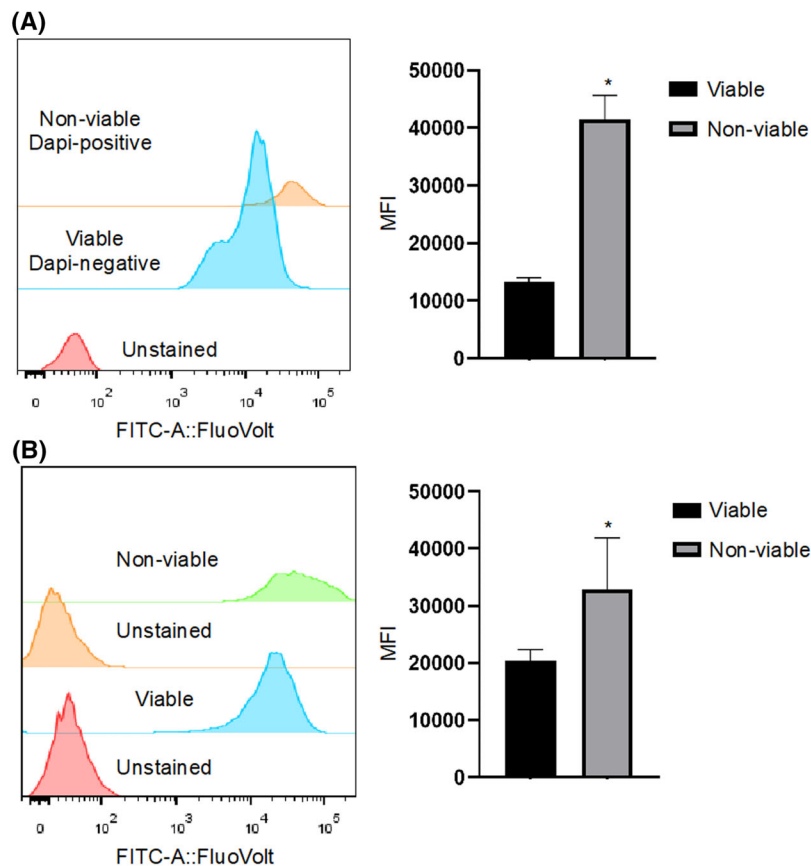


**Figure 1. Flow-cytometric measurement of the membrane potential in viable and non-viable cells.** Membrane potential measurement in T-cells in basal conditions (A) and following cell death induction (B). (A) T-cells were stained with the membrane potential sensitive fluorescent dye (FluoVolt) and the fluorescent intensity was measured in viable (DAPI-negative) and non-viable (DAPI-positive) cells. (B) Cell viability was reduced by exposing T-cells to 7 freezing/thawing cycles; cells were then stained with the membrane potential sensitive fluorescent dye (FluoVolt) and the fluorescent intensity was measured in viable (no freezing/thawing) and non-viable (7 freezing/thawing cycles) cells. Bar plots report the median fluorescence intensity (MFI) values. Data is the average of 2 (A), and 3 (B) replicates. *P* values from the two-tailed unpaired t-test are shown, *$P <$ 0.05.

conductivity of the fluid medium, $\sigma_m$, fixed at 0.420 S/m for T-cells. This $\sigma_m$ value was chosen because it led to the maximum separation between viable and non-viable cells, as resulted from the computational fluid dynamic study (see Fig. 2A later). The complete description of the model is reported in the Supporting Information.

# 3 Materials and methods

## 3.1 Materials

All chemicals were of analytical grade and used without further modification unless otherwise specified. All aqueous solutions were prepared with ultrapure water (0.182 M $\Omega$m) from a Milli-Q system (Millipore, UK). Phosphate buffer saline (PBS) solution (0.1 mM, pH 7.5, and conductivity of 0.420 S/m) was prepared to mix 1.14 g of $Na_2HPO_4$ and 0.27 g of $NaH_2PO_4$ per 100 ml of distillate water. Human T-cells were kindly provided by the human biospecimens and drug discovery services (Cambridge Bioscience Limited, Cambridge, UK). The frozen T-cell samples were placed in a hot water bath at 37°C for 5 min and then centrifuged (ALC Centrifuge PK120, Buckinghamshire, UK) at 1000 RPM for 5 min. The supernatant was removed using a micropipette and the cells are resuspended in PBS. NucleoCounter[R] NC-200[TM] was used to count the number of cells/ml of PBS.

## 3.2 Membrane potential measurement

To measure the membrane potential (potential difference between interior and exterior of the cell membrane) in T-cells, the FluoVolt Membrane Potential Kit (F10488, ThermoFisher) was used following the manufacturer's instructions. Briefly, about $2 \times 10^6$ of T-cells, cultured for 24 h in RPMI 10% FBS and 1× Glutamine, were centrifuged; the pellet was resuspended in 2 ml of staining solution and incubated for 15 min at room temperature. Next, the cells were centrifuged and washed with PBS twice (cells were centrifuged after each PBS-washing step), resuspended in 500 μL of PBS with (Figs. 1A and S1A) or without (Figs. 1B and S1B) DAPI (1 μg/ml; D9542, Sigma) and incubated for 5 min before being analyzed. The fluorescent signal from the DAPI and FluoVolt dye was measured with the BD LSR Fortessa at the wavelength of 405 nm and 488 nm, respectively. At least 10000 events were recorded for each sample. The median fluorescence intensity (MFI) was calculated over the total events (Figs. 1B and S1B) or DAPI-negative and DAPI-positive (Fig. 1A) events using the FlowJo V10 software.

## 3.3 Cell death induction and statistical analysis

To reduce cell viability, T-cells were either consecutively frozen and thawed (7 freezing/thawing cycles, performed

at the temperatures –80°C (in a freezer) and 37°C respectively by means of a water bath, Fig. 1B) or electroporated (Fig. S1B) by using the Nucleofector$^{TM}$ Device from Lonza biotech, UK (program U-014 for T cells). Afterward, cells were pelleted and processed for the staining as described above. Differences between samples were analyzed by a two-tailed unpaired t-test using GraphPad Prism 8 software (Version 8.4.3). A *P*-value lower than 0.05 was considered statistically significant.

## 3.4 Device fabrication

The cell sorter developed in this study consists of a microfluidic channel (length = 1.2 mm; width = 0.2 mm; depth = 0.05 mm; total volume = 0.012 µl), with one inlet and two outlets (each 300 µm long, 200 µm wide and 0.05 mm deep) - see Fig. S2A. An array of seven electrodes (80 µm wide, with a gap between electrodes of 80 µm), placed along one side of the microfluidic channel, allows cell separation when a voltage is applied at a set frequency.

Fig. S2 shows the several steps for the device fabrication. The microfluidic channel was fabricated by standard photolithography, followed by soft lithography. The negative photoresist SU-8 2050 (MicroChemicals GMBH, Stuttgart, Germany) was spin-coated onto a 3 inch silicon wafer (PI-KEM, Tamworth, UK) at 3000 rpm for 40 s (with the spin coater POLOS300, Miden Engweg, The Netherlands) to achieve a channel height of 40 µm (Fig. S2B). The soft baking was performed by placing the silicon wafer directly onto a hot plate at 95°C for 3 min. The inverse channel patterns were fabricated by photolithography using a mask aligner (Karl Süss, Garching, Germany). The wafer was exposed for 7 s using a UV lamp with an intensity of 9.4 mN/cm$^2$. A development step was performed to remove the access photoresist using SU-8 developer (MicroChemicals GMBH, Stuttgart, Germany). The structure was replicated in polydimethylsiloxane (PDMS) (Sylgard 184, Dow Corning, US), prepared with a 10:1 (base: crosslinker) ratio, which was poured onto the silicon wafer containing the channel inverse pattern and cured at 75°C for 60 minutes (Fig. S2C). The resulting structure, peeled off from the silicon wafer, was bonded to the glass slide with the patterned electrodes by using an oxygen plasma at 100 W for 45 s (Zepto plasma system, Diner GMBH, Germany), as shown in Fig. S2A. Fig. S2E shows an actual photo of the whole device.

The electrodes array was fabricated by spin-coating the negative photoresist Az2020 (MicroChemicals GMBH, Stuttgart, Germany), at 3000 rpm and for 30 s, onto a glass slide; exposing the resulting glass slide to UV (intensity 9.4 mN/cm$^2$) for 2 s; and incubating it for 2 min with a Az826 MIF developer (MicroChemicals GMBH, Stuttgart, Germany).

A 40 nm titanium adhesion layer was deposited by thermal evaporation at 1400°C onto the patterned glass slide (Edwards coating system E306A), followed by a 200 nm gold (Au) layer (Fig. S2D). Subsequently, the glass slide was immersed in a petri dish of acetone for 5 min to liftoff the unpolymerised photoresist, leaving the patterned electrodes only. The resulting structure was rinsed with DI water and dried before sealing the PDMS channel on top of the electrode array by plasma bonding.

## 3.5 Experimental setup

The separation efficacy of the microfluidic chip was assessed with the help of an inverted microscope (Olympus IX73), equipped with a CCD camera (Olympus XM10). Human T-cells were used, at a cell population of $0.6 \times 10^6$ cells/ml in PBS, with a conductivity of 0.420 S/m. PBS containing T-cells was injected into the microfluidic chip with a syringe pump (World Precision Instrument NE200) at a flow rate of 20 µl/h. A waveform generator (TENMA 72–3555), connected to the electrodes array via copper wires and a conductive paste, was used to apply an AC field with a frequency within the range of 10 KHz–3 MHz, and sort T-cells according to their dielectric properties, as shown in Fig. S3. High-quality images were acquired every 7 s by using the CCD camera. The schematic of the experimental setup is shown in Fig. S4.

Viable and non-viable cells at a 1:1 ratio (fixed concentration for each type of cells: $0.6 \times 10^6$ cells/ml) were fed into the device over five hours. A sample volume of 60 µl was collected (resuspended by pipetting) from the reservoirs connected to the two outlets, and the cell viability of the feeding suspension and the two outlets, resuspended by pipetting, was investigated by using a NucleoCounterR NC-200TM. The latter was also used to assess the cell density in both outlets [50], equal to $0.59 \times 10^6$ cells/ml, suggesting a loss of $1 \times 10^4$ cells/ml during each experiment.

The efficacy of separation of the chip was assessed on the basis of:

1. the degree of purity of viable cells in the top outlet, which provides an indication on the presence of harmful non-viable cells in this stream, % $\textit{Purity} = \frac{N_{v\_T}}{N_{tot\_T}} \times 100\%$, where Nv_T refers to the number of viable cells in the top outlet, and Ntot_T refers to the total number of cells in the top outlet.
2. the yield of separation, which provides an indication of loss of viable cells in the bottom outlet, % $\textit{Yield} = \frac{N_{v\_T}}{N_{v\_tot}} \times 100\%$, where Nv_tot refers to the number of viable cells in the inlet.

## 4 Results and discussion

### 4.1 Measuring the membrane potential

Membrane potential in cells controls essential biological processes, ranging from contractility to cell cycle control and cancer progression [51,52]. Cell death has been associated with a change in plasma membrane potential (PMP), which

is mainly caused by a change of intracellular potassium and sodium [53,54].

First, to assess the potential effectiveness of a DEP-based separation, the PMP dielectric properties of both viable and non-viable human T-cells were quantified and compared. The advantage was taken of the natural cell death process, which takes place after cells are cultured for a certain time. The T-cells were kept in culture conditions for 24 h, after which they were stained with a membrane potential-sensitive fluorescent dye. This step enabled the measurement of fast changes in the membrane potential, PMP, which were analyzed using flow-cytometry [55]. Based on the incorporation of DAPI [56,57], a cell viability-sensitive dye, the PMP was measured on both viable (DAPI-negative fraction) and non-viable (DAPI-positive fraction) cells (Fig. 1A and S1A). A significant increase in the fluorescent intensity from non-viable cells incubated with the membrane potential sensitive dye was found, indicating membrane depolarisation due to the influx of positively charged ions (Fig. 1A) [58]. Next, we measured the membrane potential of T-cells with cell viability experimentally reduced via multiple freezing/thawing cycles (Fig. 1B) or electroporation (Fig. S1B). As for DAPI-positive cells in Fig. 1A, this experiment showed a significant increase in plasma membrane depolarisation when cell viability was reduced (Figs. 1B and S1B).

These results confirm that the membrane potential of T-cells changes according to the viability, and that the dielectric property can be used for discriminating viable and non-viable cells, motivating the development of DEP-based platforms for the separation and enrichment of viable cells.

## 4.2 Optimal operational parameters for effective cell sorting

To successfully separate the T-cells with different dielectric properties by dielectrophoresis, their $K$ factor should be different at a fixed frequency [59,60]. To quantify the dielectric response of T-cells under an applied electric field, the $K$ factor for viable and non-viable T-cells was calculated as a function of frequency by using Equation (5). The results, only concerning the real part of $K$, are shown in Fig. S5. The plots were generated by keeping all the dielectric parameters of the T-cells constant and changing the frequency of the applied electric field for three different values of conductivity of the media, $\sigma_m$.

The value of $K$ is in line with previous studies [45,61], and for both viable and non-viable T-cells changes according to the value of the medium conductivity ($\sigma_m$), as shown in Fig. S5. These trends are in agreement with recent studies on yeast [41] and HEK 293 cells [42].

For $\sigma_m = 0.02$ S/m and under low frequencies ($1.5 \times 10^2$–$1.5 \times 10^4$ Hz), viable cells demonstrate a negative DEP behavior, with a $K$ factor of –0.27 (Fig. 2A). This behavior is caused by the Maxwell-Wagner polarisation of the interface between the cell membrane and the surrounding solution [62]. The critical frequency, where the cells first change
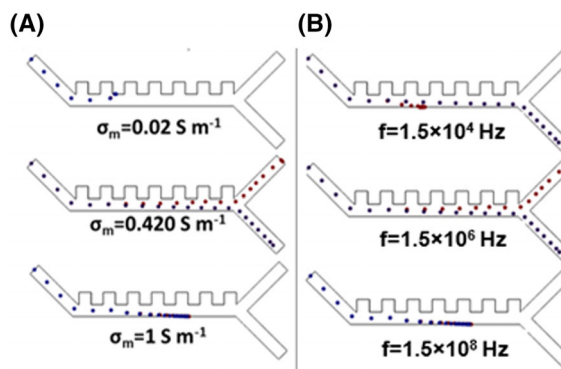


**Figure 2.** Simulation of viable and non-viable T-cells separation over time by DEP in the microfluidic device developed. T-cell separation under: A) three different values of conductivity of the suspended medium, 0.02 S/m, 0.42 S/m, 1 S/m, for $f = 1.5 \times 10^6$ Hz, $V$pp = 5 V, and a flow rate of 20 µl/h; B) three different values of frequency, $1.5 \times 10^4$ Hz, $1.5 \times 10^6$ Hz, $1.5 \times 10^8$ Hz, at $\sigma_m = 0.420$ S/m. In the simulation, viable and non-viable cells are represented with red and blue circles, respectively.

their DEP response from negative to positive or vice versa, is known as the first cross-over frequency [63,64]. According to Fig. S5A, the first cross-over frequency result to be approximately $1.5 \times 10^5$ Hz. As the frequency increases to $1.5 \times 10^6$ Hz, the cells experience positive DEP with a $K$ factor of 0.87, to then transit back to a negative DEP region when the frequency is further increased to $1.5 \times 10^8$ Hz. On the other hand, under a conductivity of 0.02 S/m, non-viable cells remain in the positive DEP region thorough the whole frequency range.

When the conductivity is increased to 0.420 S/m, viable cells experience negative DEP for frequencies between $1.5 \times 10^2$ Hz and $1.5 \times 10^4$ Hz, with a $K$ factor of –0.48 (Fig. S5B). The transition to the positive DEP region for these cells occurs when the applied AC frequency is increased to $1.5 \times 10^6$ Hz with a $K$ factor of 0.01. The viable T-cells cross back to the negative DEP region at $1.5 \times 10^8$ Hz and remain in the negative DEP region for the rest of the frequency range. In this case, non-viable cells experience a negative DEP throughout the frequency range (Fig. S5B). As shown in Fig. S5C, when the conductivity of the media is further increased to 1 S/m, both viable and non-viable T-cells undergo a negative DEP response for the entire frequency range tested [65–67]. The cells response to DEP at frequencies higher than the first cross-over frequency is governed by the interaction between cell cytoplasm and suspending solution [68,69]. On the contrary, at frequencies lower than the first cross-over frequency, the interaction between the cell membrane and the medium determines the dielectric response of the cells [41]. Based on these results, computational fluid dynamic studies were performed on single cell for three $\sigma_m$ values to identify the optimal values of conductivity and frequency for effective cells separation in the microfluidic device. Initially, the numerical simulations were set by applying an AC field at a frequency of $1.5 \times 10^6$ Hz, which, as shown in Fig. S5, is higher than the estimated first cross-over frequency. The results are shown in Fig. 2A.

Under the lowest conductivity value investigated, both viable ($\sigma_{\text{cytoplasm}} = 0.56$ S/m) and non-viable ($\sigma_{\text{cytoplasm}} = 0.27$ S/m) T-cells are more polarisable and move closer to the electrode array at the top of the microfluidic channel, as a result of the higher cytoplasmic conductivities compared to the fluid medium surrounding the cells [70]. When the medium conductivity is increased to 0.420 S/m, while keeping all the other parameters unchanged, the viable cells are pushed toward the top outlet, since they are more polarisable than the surrounding medium (pDEP). Contrary, the non-viable cells, less polarisable than the surrounding medium (nDEP), move away from the electrode array toward the bottom outlet. As the medium conductivity is further increased to 1 S/m, both viable and non-viable cells become less polarisable and experience nDEP, thus moving away from the electrode array (bottom outlet). Finally, the effect of the applied dielectrophoretic force, $F_{\text{DEP}}$, on the cell separation efficacy was investigated by keeping the medium conductivity constant at 0.420 S/m (Fig. 2B). At $1.5 \times 10^4$ Hz, both viable ($\sigma_{\text{mem}} = 6.63 \times 10^{-6}$ S/m) and non-viable ($\sigma_{\text{mem}} = 6.63 \times 10^{-2}$ S/m) cells become less polarisable than the medium in which they are suspended and move away from the electrode array and toward the bottom outlet, experiencing nDEP. Fig. 2B shows that, at $1.5 \times 10^6$ Hz, viable T-cells ($\sigma_{\text{cytoplasm}} = 0.56$ S/m) experience pDEP and move closer to the electrode array, while non-viable T-cells ($\sigma_{\text{cytoplasm}} = 0.27$ S/m) move away from the electrode, due to nDEP.

The DEP response of the cells at frequencies higher than the second cross-over frequency is governed by the interaction of cells cytoplasmic dielectric permittivity and the permittivity of the surrounding medium. The second cross-over frequency for $\sigma_m = 0.420$ S/m is estimated to be $1.5 \times 10^7$ Hz from Fig. S5B. Under this frequency, both the viable and non-viable cells ($\epsilon_{\text{cytoplasm viable}} = 70$ $\epsilon_{\text{cytoplasm nonviable}} = 50$) experience nDEP and move away from the electrode array as their $\epsilon_{\text{cytoplasm}}$ is less than the $\epsilon_{\text{medium}} = 80$.

These results validate the analytical results presented in Fig. S5. The analytical and computational fluid dynamics results presented in these sections formed the basis of our platform design and experimental results.

## 4.3 Validating the separation efficacy

The optimal operational parameters resulting from the simulation analysis, within the range tested, were subsequently validated with the fabricated device. Viable and non-viable T-cells with a ratio of 1:1 suspended in PBS ($\sigma_m = 0.420$ S/m) at a concentration of $0.6 \times 10^6$ cells/ml were injected into the device at 20 µl/h. As predicted, under an applied frequency of $1.5 \times 10^4$ Hz, both viable and non-viable cells experienced nDEP and moved away from the region of high electric field strength toward the bottom outlet (Fig. 3A). When the frequency was increased to $1.5 \times 10^6$ Hz, the viable cells experienced pDEP, with *K* factor of 0.016, and moved toward the top outlet. The non-viable cells, on the other hand, experienced
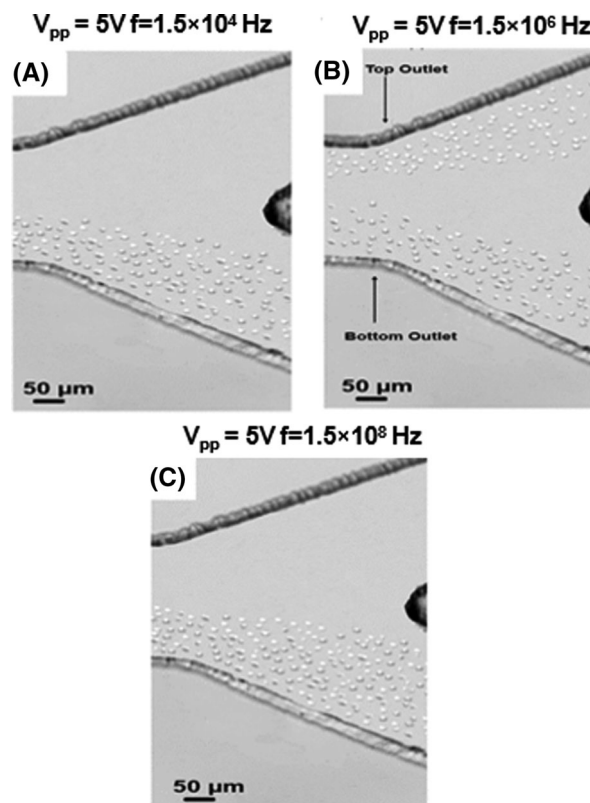


**Figure 3**. Microscope images of T-cells in the microfluidic device during operation under a flow rate of 20 µl/h and an applied voltage ($V_{\text{p-p}}$) of 5 V. The images were recorded at 7 fps at a magnification of 10x. (A) Viable and non-viable T-cells moving toward the bottom outlet, the region of low electric field (nDEP). (B) Viable T-cells moving toward region of high electric field strength, closer to the electrode arrays at the top outlet (pDEP) and non-viable cells move toward the bottom outlet. (C) Viable and non-viable T-cells moving toward the bottom outlet, the region of low electric field (nDEP).

nDEP with a *K* factor value of –0.07 and moved to the bottom outlet (Fig. 3B).

As shown in Fig. 3, viable cells are visually different from non-viable cells as the latter have a degraded and permeable outer membrane, which gives them a unique shape [24,71]. At a frequency of $1.5 \times 10^6$ Hz, the separation between viable and non-viable T-cells is not binary and some of the viable T-cells move toward the bottom outlet. As the frequency is further increased to $1.5 \times 10^8$ Hz, both viable and non-viable cells enter the nDEP region and move toward the bottom outlet (Fig. 3C). These experimental results validate the mathematical simulations on the applied frequency for effectively sorting viable and non-viable CAR-T cells. Under an applied AC frequency of $1.5 \times 10^6$ Hz, which, according to our results corresponded to the optimal condition for separation, a purity of 96% in the top outlet was observed, with a yield of separation of 93%. The separation efficacy of our device is in line with previous examples of DEP-based microfluidic devices; while values of purity as high as 99% [72] for viable and non-viable yeast cells, and 98.8% to separate red blood

cells from platelets [45], have been reported, most studies report values of purity within the range 95–97% [32,43,73,74]. Methods of separation of viable and non-viable cells based on mechanical forces are characterized by a lower purity, within the range 70–85% [24,75]. In all the above-mentioned devices, a decrease in the sorting efficiency at higher flow rates is observed [24,43,73,74]. As such, the effect of different flow rates on the sorting efficiency of our device was quantified. To achieve this, a 1:1 mixture of viable and non-viable cells ratio (each at a concentration of $0.6 \times 10^6$ cells/ml) was injected into the system. The flow rate was increased from 20 µl/h to $2 \times 10^4$ µl/h in steps of 200 µl/h. As shown in Fig. S6, by increasing the flow rate to $2 \times 10^4$ µl/h, the average efficiency decreased to 86% when the flow rate was $2 \times 10^3$ µl/h and to 80% at $2 \times 10^4$ µl/h. The decrease in sorting efficiency at high flow rates in our device is attributed to the absence of hydrodynamic focusing inlet (single inlet) reported in earlier devices and has been discussed previously [76]. It was also noted that, at high flow rates, cells experienced high shear rates and it became increasingly difficult to visualize them during experiments as shown in Fig. S7.

## 5 Concluding remarks

In this study, we present a novel AC-dielectrophoretic single-inlet microfluidic device for continuous separation of T-cells according to their viability, characterized by a simple operation compatible with continuous applications and no need for additional reagents. An AC electric field is applied via an array of castellated microelectrodes embedded into a single microfluidic channel to separate online flowing cells based on their dielectric properties. First, to support the design of an effective device, the separation efficacy of the device was mathematically simulated under a range of applied AC frequency and for several values of conductivity of the medium. It resulted that, within the range tested, the optimal values of applied AC frequency and media conductivity are respectively $1.5 \times 10^6$ Hz and 0.420 S/m. Under these operational conditions, the separation of viable and non-viable T-cells was experimentally validated. A separation efficiency of 93%, under a flow rate of 20 µl/h, was demonstrated. This study provides the first example of on-chip continuous separation of T-cells according to their viability, which can protect patients from the detrimental effects of infusion with non-viable cells. It consequently represents a milestone toward the development of lab-on-a-chip devices for point-of-need and cost-effective T-cell-based personalised therapies.

*The authors have declared no conflict of interest.*

## Data availability statement

The data that support the findings of this study are available from the corresponding author upon reasonable request.

## 6 References

[1] Sharma, P., Hu-Lieskovan, S., Wargo, J. A., Ribas, A., *Cell* 2017, *168*, 707–723.

[2] Miliotou, A. N., Papadopoulou, L. C., *Curr. Pharm. Biotechnol.* 2018, *19*, 5–18.

[3] Panagopoulou, T. I., Rafiq, Q. A., *Biotechnol. Adv.* 2019, *37*, 107411.

[4] Wang, X., Rivière, I., *Mol. Ther. Oncolytics* 2016, *3*, 16015.

[5] Zhang, Z., Qiu, S., Zhang, X., Chen, W., *BMC Biotechnol.* 2018, *18*, 4.

[6] Gang-Ming, Z., *J. Cell. Physiol.* 2007, *213*, 440–444.

[7] Titov, A., Petukhov, A., Staliarova, A., Motorin, D., Bulatov, E., Shuvalov, O., Soond, S. M., Piacentini, M., Melino, G., Zaritskey, A., Barlev, N. A., *Cell Death Dis.* 2018, *9*, 897.

[8] Vedvyas, Y., McCloskey, J. E., Yang, Y., Min, I. M., Fahey, T. J., Zarnegar, R., Hsu, Y. M. S., Hsu, J. M., Besien, K. V, Gaudet, I., Law, P., Kim, N. J., Hofe, E., Jin, M. M., *Sci. Rep.* 2019, *9*, 10634.

[9] Környei, Z., Beke, S., Mihálffy, T., Jelitai, M., Kovács, K. J., Szabó, Z., Szabó, B., *Sci. Rep.* 2013, *3*, 1088.

[10] Mishra, S. R., Thakur, N., Somal, A., Parmar, M. S., Reshma, R., Rajesh, G., Yadav, V. P., Bharti, M. K., Bharati, J., Paul, A., Chouhan, V. S., Sharma, G. T., Singh, G., Sarkar, M., *Res. Vet. Sci.* 2016, *108*, 98–111.

[11] Moss, L. D., Monette, M. M., Jaso-Friedmann, L., Leary, J. H., Dougan, S. T., Krunkosky, T., Evans, D. L., *Dev. Comp. Immunol.* 2009, *33*, 1077–1087.

[12] Nybo, K., *BioTechniques* 2014, *56*, 59.

[13] Liao, X., Makris, M., Luo, X. M., *J. Vis. Exp.* 2016, *2016*, 54641.

[14] Basu, S., Campbell, H. M., Dittel, B. N., Ray, A., *J. Vis. Exp.* 2010, 3–6.

[15] Shen, Y., Yalikun, Y., Tanaka, Y., *Sens. Actuators B* 2019, *282*, 268–281.

[16] Huh, D., Bahng, J. H., Ling, Y., Wei, H. H., Kripfgans, O. D., Fowlkes, J. B., Grotberg, J. B., Takayama, S., *Anal. Chem.* 2007, *79*, 1369–1376.

[17] Laurell, T., Petersson, F., Nilsson, A., *Chem. Soc. Rev.* 2007, *36*, 492–506.

[18] Wu, M., Ozcelik, A., Rufo, J., Wang, Z., Fang, R., Jun Huang, T., *Microsystems Nanoeng.* 2019, *5*, 32.

[19] Sang, B. K., Sang, Y. Y., Hyung, J. S., Sang, S. K., *Anal. Chem.* 2008, *80*, 2628–2630.

[20] Atajanov, A., Zhbanov, A., Yang, S., *Micro Nano Syst. Lett.* 2018, *6*, 2.

[21] Pamme, N., *Lab Chip* 2006, *6*, 24–38.

[22] Zborowski, M., Chalmers, J. J., *Anal. Chem.* 2011, *83*, 8050–8056.

[23] Halagačka, L., Postava, K., Vanwolleghem, M., Vaurette, F., Ben Youssef, J., Dagens, B., Pištora, J., *Opt. Mater. Express* 2014, *4*, 1903–1919.

[24] Islam, M., Brink, H., Blanche, S., DiPrete, C., Bongiorno, T., Stone, N., Liu, A., Philip, A., Wang, G., Lam, W., Alexeev, A., Waller, E. K., Sulchek, T., *Sci. Rep.* 2017, *7*, 1997.

[25] Fu, A. Y., Spence, C., Scherer, A., Arnold, F. H., Quake, S. R., *Nat. Biotechnol.* 1999, *17*, 1109–1111.

[26] Gossett, D. R., Weaver, W. M., Mach, A. J., Hur, S. C., Tse, H. T. K., Lee, W., Amini, H., Di Carlo, D., *Anal. Bioanal. Chem.* 2010, *397*, 3249–67.

[27] Tottori, N., Nisisako, T., Park, J., Yanagida, Y., Hatsuzawa, T., *Biomicrofluidics* 2016, *10*, 014125.

[28] Jo, Y., Shen, F., Hahn, Y. K., Park, J. H., Park, J. K., *Micromachines* 2016, *7*, 1–9.

[29] Di Carlo, D., *Lab Chip* 2009, *9*, 3038–3046.

[30] Rahman, N. A., Ibrahim, F., Yafouz, B., *Sensors* 2017, *17*, 449.

[31] RC, G. P., Jody, V., *Electrophoresis* 2002, *23*, 1973–1983.

[32] Doh, I., Cho, Y. H., *Sens. Actuators A* 2005, *121*, 59–65.

[33] Cheng, I. F., Chang, H. C., Hou, D., Chang, H. C., *Biomicrofluidics* 2007, *1*, 21503.

[34] Pethig, R., *Biomicrofluidics* 2010, *4*, 022811.

[35] Patel, S., Showers, D., Vedantam, P., Tzeng, T. R., Qian, S., Xuan, X., *Biomicrofluidics* 2012, *6*, 034102.

[36] Yildizhan, Y., Erdem, N., Islam, M., Martinez-Duarte, R., Elitas, M., *Sensors* 2017, *17*, 2691.

[37] Li, H., Bashir, R., *Sens. Actuators B* 2002, *86*, 215–221.

[38] Li, Y., Dalton, C., Crabtree, H. J., Nilsson, G., Kaler, K. V. I. S., *Lab Chip* 2007, *7*, 239–248.

[39] Tran, T. S. H., Ho, B. D., Beech, J. P., Tegenfeldt, J. O., *Lab Chip* 2017, *17*, 3592–3600.

[40] Beech, J. P., Keim, K., Ho, B. D., Guiducci, C., Tegenfeldt, J. O., *Adv. Mater. Technol.* 2019, *4*, 1900339.

[41] Zhao, K., Larasati, Duncker, B. P., Li, D., *Anal. Chem.* 2019, *91*, 6304–6314.

[42] Wei, Z., Li, X., Zhao, D., Yan, H., Hu, Z., Liang, Z., Li, Z., *Anal. Chem.* 2014, *86*, 10215–10222.

[43] Braschler, T., Demierre, N., Nascimento, E., Silva, T., Oliva, A. G., Renaud, P., *Lab Chip* 2008, *8*, 280–286.

[44] Demierre, N., Braschler, T., Muller, R., Renaud, P., *Transducers Eurosensors '07 - 4th Int. Conf. Solid-State Sensors, Actuators Microsystems* 2007, *132*, 1777–1780.

[45] Piacentini, N., Mernier, G., Tornay, R., Renaud, P., *Biomicrofluidics* 2011, *5*, 034122–034122-8.

[46] Adams, T. N. G., Turner, P. A., Janorkar, A. V., Zhao, F., Minerick, A. R., *Biomicrofluidics* 2014, *8*, 054109.

[47] Wu, L., Lanry Yung, L. Y., Lim, K. M., *Biomicrofluidics* 2012, *6*, 014113.

[48] Polevaya, Y., Ermolina, I., Schlesinger, M., Ginzburg, B. Z., Feldman, Y., *Biochim. Biophys. Acta Biomembr.* 1999, *1419*, 257–271.

[49] Liu, W., Ren, Y., Tao, Y., Zhou, Z., Wu, Q., Xue, R., Yao, B., *J. Phys. D. Appl. Phys.* 2020, *53*, 175304.

[50] Xiong, K., Marquart, K. F., la Cour Karottki, K. J., Li, S., Shamie, I., Lee, J. S., Gerling, S., Yeo, N. C., Chavez, A., Lee, G. M., Lewis, N. E., Kildegaard, H. F., *Biotechnol. Bioeng.* 2019, *116*, 1813–1819.

[51] Belle, M. D. C., Diekman, C. O., Forger, D. B., Piggins, H. D., *Science* 2009, *326*, 281–284.

[52] Maxwell, R. B., Gerhardt, A. L., Toner, M., Gray, M. L., Schmidt, M. A., 2003, *12*, 630–640.

[53] Bortner, C. D., Hughes, F. M., Cidlowski, J. A., *J. Biol. Chem.* 1997, *272*, 32436–32442.

[54] Dallaporta, B., Hirsch, T., Susin, S. A., Zamzami, N., Larochette, N., Brenner, C., Marzo, I., Kroemer, G., *J. Immunol.* 1998, *160*, 5605–5615.

[55] Perfetto, S. P., Chattopadhyay, P. K., Lamoreaux, L., Nguyen, R., Ambrozak, D., Koup, R. A., Roederer, M., *Curr. Protoc. Cytom.* 2010, *53*, 9.34.1–9.34.14.

[56] Villas, B. H., *Cell Vis.* 1998, *5*, 56–61.

[57] Johnson, S., Nguyen, V., Coder, D., *Curr. Protoc. Cytom.* 2013, *64*, 9.2.1–9.2.26.

[58] Adams, D. S., Levin, M., *Cold Spring Harb Protoc.* 2012, *2012*, 459–464.

[59] Lo, Y. J., Lin, Y. Y., Lei, U., Wu, M. S., Yang, P. C., *Appl. Phys. Lett.* 2014, *104*, 083701.

[60] Lo, Y. J., Lei, U., *Electrophoresis* 2020, *41*, 137–147.

[61] Ohta, A. T., Chiou, P. Y., Phan, H. L., Sherwood, S. W., Yang, J. M., Lau, A. N. K., Hsu, H. Y., Jamshidi, A., Wu, M. C., *IEEE J. Sel. Top. Quantum Electron.* 2007, *13*, 235–242.

[62] Sun, T., Morgan, H., *Microfluid. Nanofluidics* 2010, *8*, 423–443.

[63] Weng, P. Y., Chen, I. A., Yeh, C. K., Chen, P. Y., Juang, J. Y., *Biomicrofluidics* 2016, *10*, 011909.

[64] Lu, Y. W., Sun, C., Kao, Y. C., Hung, C. L., Juang, J. Y., *Nanomaterials* 2020, *10*, 1364.

[65] Castellarnau, M., Errachid, A., Madrid, C., Juárez, A., Samitier, J., *Biophys. J.* 2006, *91*, 3937–3945.

[66] Thomas, R. S., Morgan, H., Green, N. G., *Lab Chip* 2009, *9*, 1534–1540.

[67] Elvington, E. S., Salmanzadeh, A., Stremler, M. A., Davalos, R. V., *J. Vis. Exp.* 2013, https://doi.org/10.3791/50634.

[68] Gascoyne, P. R. C., Shim, S., *Cancers* 2014, *6*, 545–579.

[69] Yang, G., Sau, C., Lai, W., Cichon, J., Li, W., 2015, *344*, 1173–1178.

[70] Liang, W., Yang, X., Wang, J., Wang, Y., Yang, W., Liu, L., *Micromachines* 2020, *11*, 513.

[71] Zhang, Y., Chen, X., Gueydan, C., Han, J., *Cell Res.* 2018, *28*, 9–21.

[72] Mernier, G., Braschler, T., Renaud, P., *Lab Chip* 2010, *10*, 2077–2082.

[73] Lee, D., Hwang, B., Kim, B., *Micro Nano Syst. Lett.* 2016, *4*, 2.

[74] Jiang, A. Y. L., Yale, A. R., Aghaamoo, M., Lee, D. H., Lee, A. P., Adams, T. N. G., Flanagan, L. A., *Biomicrofluidics* 2019, *13*, 064111.

[75] Sajeesh, P., Raj, A., Doble, M., Sen, A. K., *RSC Adv.* 2016, *6*, 74704–74714.

[76] Yang, J., Huang, Y., Wang, X. B., Becker, F. F., Gascoyne, P. R. C., *Biophys. J.* 2000, *78*, 2680–2689.